Organosilica nanoparticles functionalised with p-anisaldehyde and p-chlorobenzaldehyde Schiff bases: synthesis, physicochemical properties, toxicological and antimicrobial evaluation

Biomaterials Advances 184 (2026) 214795

Contents lists available at ScienceDirect

Biomaterials Advances

journal homepage: www.journals.elsevier.com/materials-science-and-engineering-c

Organosilica nanoparticles functionalised with p-anisaldehyde and p-chlorobenzaldehyde Schiff bases: Synthesis, physicochemical properties, toxicological and antimicrobial evaluation☆

Zhansaya E. Kozhantayeva [a], Gemma Walton [b], Galiya S. Irmukhametova [a,**], Vitaliy V. Khutoryanskiy [c,d,*]

[a] Department of Chemistry and Chemical Technology, Al-Farabi Kazakh National University, 050040, Almaty, Kazakhstan
[b] Department of Food and Nutritional Sciences, University of Reading, Whiteknights, RG6 6DX, Reading, United Kingdom
[c] Reading School of Pharmacy, University of Reading, Whiteknights, RG6 6DX, Reading, United Kingdom
[d] Physicochemical, Ex Vivo and Invertebrate Tests and Analysis Centre (PEVITAC), University of Reading, Reading, RG6 6AD, United Kingdom

ARTICLE INFO

Keywords:
Organosilica nanoparticles
Schiff bases
Polyethylene glycol
Surface modification, antimicrobial activity

ABSTRACT

In this study, bifunctional organosilica nanoparticles bearing thiol and amine functionalities were synthesized, PEGylated, and subsequently functionalised with aromatic aldehydes via Schiff base formation. The nanoparticles were prepared by an Ouzo effect–based nanoprecipitation method using 3-mercaptopropyltrimethoxysilane and 3-aminopropyltrimethoxysilane as precursors. Comprehensive physicochemical characterisation was performed using dynamic light scattering, nanoparticle tracking analysis, transmission electron microscopy, ζ-potential measurements, Ellman's and 4-nitrobenzaldehyde assays, FTIR spectroscopy, and X-ray diffraction. PEGylation markedly improved colloidal stability, resulting in aggregation-free dispersions across a broad pH range. In vivo toxicological assessment using *Schmidtea mediterranea* planaria demonstrated good biocompatibility of all nanoparticle formulations, with no evidence of epithelial barrier disruption. Antimicrobial activity was evaluated in vitro against *Staphylococcus aureus*. Nanoparticles functionalised with aromatic aldehydes exhibited pronounced antibacterial activity, whereas PEGylated nanoparticles showed only weak effects and non-functionalised nanoparticles were inactive.

1. Introduction

The development of silica-based nanoparticles has attracted considerable attention due to their exceptional stability, tunable physicochemical properties, and wide-ranging applications in biomedical and pharmaceutical sciences [1]. Their ability to efficiently encapsulate therapeutic agents, enhance bioavailability, and facilitate targeted drug delivery makes them highly promising in modern nanomedicine. Moreover, the U.S. Food and Drug Administration (FDA) has recognized certain commonly used forms of silica (e.g., silicon dioxide) as generally safe for biomedical applications [2]. A key advantage of these nanoparticles lies in their high surface area and ease of modification, which enable precise tuning of their properties for specific therapeutic and diagnostic applications [3].

Silica nanoparticles offer exceptional versatility due to the high density of surface functional groups that are possible to chemically modify, enabling easy functionalization with various chemical groups such as amines (-NH_2), thiols (-SH), and carboxyls (-COOH). The presence of silanol groups on their surface facilitates bioconjugation, improving their interaction with biomolecules and enhancing their potential in targeted drug delivery. Furthermore, their size and morphology can be finely controlled by adjusting synthesis parameters, including precursor concentration, catalyst type, pH, and reaction temperature [4,5]. While physical adsorption is the most common approach for drug loading onto silica nanoparticles [6], recent studies have demonstrated that covalent binding strategies can significantly

☆ This article is part of a Special issue entitled: 'UKSB2025' published in Biomaterials Advances.

* Correspondence to: V.V. Khutoryanskiy, Reading School of Pharmacy, University of Reading, Whiteknights, RG6 6DX Reading, United Kingdom.
** Correspondence to: G.S. Irmukhametova, Department of Chemistry and Chemical Technology, Al-Farabi Kazakh National University, 050040, Almaty, Kazakhstan.
E-mail addresses: galiya.irm@gmail.com (G.S. Irmukhametova), v.khutoryanskiy@reading.ac.uk (V.V. Khutoryanskiy).

https://doi.org/10.1016/j.bioadv.2026.214795
Received 25 December 2025; Received in revised form 16 February 2026; Accepted 26 February 2026
Available online 5 March 2026

improve drug-loading efficiency and release kinetics [7].

In particular, amino-functionalized mesoporous organosilica nanoparticles have shown enhanced drug encapsulation and pH-responsive release, making them promising candidates for controlled drug delivery applications [8]. An important advancement in this field is the development of degradable mesoporous organosilica nanoparticles (MONs), which address concerns related to long-term accumulation in biological systems. By incorporating biodegradable linkages into the silica framework, MONs undergo controlled degradation under physiological conditions, ensuring efficient drug release while minimizing potential toxicity [9]. These advances emphasize the growing potential of functionalized silica-based nanoplatforms for biomedical applications, including targeted therapy, bioimaging, and controlled drug release [10].

Our research group has conducted extensive studies on thiolated organosilica nanoparticles, including their synthesis, size control, and biomedical applications [11–14]. We demonstrated that solvent polarity, catalyst type, and temperature markedly affect nanoparticle size and surface properties [13], and confirmed the in vitro and in vivo biocompatibility of thiolated and PEGylated organosilica nanoparticles [14]. It was also demonstrated that thiolated silica nanoparticles exhibit mucoadhesive properties, enabling prolonged mucosal retention via thiol-mediated interactions [15].

The escalating problem of antimicrobial resistance and the limited pipeline of new antibiotics highlight the urgent need for novel antimicrobial formulations [16,17]. Nanoparticle-based systems with intrinsic or enhanced antimicrobial activity can improve drug stability, targeted delivery, and local retention at infection sites. This may increase efficacy, lower required doses, and help limit resistance development, making antimicrobial nanoparticles a promissing next-generation anti-infective strategy [18,19]. Literature suggests that nanomaterials bearing bioactive groups can kill bacteria via direct contact; amine-functional nanostructures, in particular, can electrostatically interact with negatively charged bacterial cell wall components [20,21]. These contact-dependent mechanisms are especially relevant for Gram-positive pathogens such as *Staphylococcus aureus*, which readily adhere to surfaces and form biofilms [22]. *Staphylococcus aureus* is one of the major causative agents of skin, wound, and mucosal infections in humans and is widely used as an model microorganism for evaluating novel antimicrobial materials due to its high propensity for developing antibiotic resistance [23].

Functional silica nanoparticles are a valuable platform for antimicrobial materials; here we introduce a modular organosilica nanoparticle design that combines thiol/amine co-condensation, PEGylation, and adjustable aromatic Schiff-base surface functionalisation within a single construct. Organosilica nanoparticles were synthesized from 3-mercaptopropyltrimethoxysilane and 3-aminopropyltrimethoxysilane, followed by surface PEGylation and further functionalisation via Schiff base formation with p-anisaldehyde and p-chlorobenzaldehyde. The resulting nanoparticles were comprehensively characterised in terms of their physicochemical properties, preliminary toxicological profile, and in vitro antimicrobial activity against *Staphylococcus aureus* NCTC 10788.

2. Materials and methods

2.1. Materials

3-Mercaptopropyltrimethoxysilane (MPTS), 3-aminopropyltrimethoxysilane (APTS), methoxypolyethylene glycol maleimide (MePEG, ≥90% by NMR, MW 5000), 5,5′-dithiobis(2-nitrobenzoic acid) (DTNB, ≥98%), and cysteine hydrochloride, benzalkonium chloride (BAC), 4-nitrobenzaldehyde (NBA), nutrient agar, fluorescein sodium salt (NaFl), resazurin sodium salt, dialysis tubing cellulose membrane (MWCO 12–14 kDa, flat width 43 mm), diethylenetriaminepentaacetic acid (DTPA) were purchased from Sigma-Aldrich (UK), and used without further purification. 4-Anisaldehyde (AA, 98%) was obtained from Sigma-Aldrich (Bangalore, India). Dimethyl sulfoxide (DMSO), nutrient broth and sodium hydroxide were obtained from Thermo Fisher (UK).

2.2. Synthesis of bifunctional silica nanoparticles

The synthesis of bifunctional silica nanoparticles was adapted from Chiu [24]. Briefly, an organic phase consisting of 8.13 mL of DMSO, 0.37 mL of MPTMS/APTS (varied ratios, total 200 mM), 0.5 mL of 10 mM diethylenetriaminepentaacetic acid (DTPA), and 1 mL of 5 M HCl was prepared. The solution was equilibrated in an ice bath for 10 min, then incubated at room temperature in the dark for 24 h. Following this, 1 mL of the organic phase was injected into 10 mL of water under stirring at 300 rpm at room temperature. The resulting colloidal dispersion was aged at 60 °C for 2 h and then purified by dialysis against deionised water (5 L; MWCO 12000–14,000 Da; eight water changes) for 48 h to remove salts and unreacted monomers. The purified nanoparticles were stored at 4 °C in aqueous dispersions.

2.3. PEGylation of nanoparticles

10 mL of the aqueous nanoparticle dispersion (1.2 mg/mL) was mixed with 50 mg of methoxy–polyethylene glycol maleimide, after which the reaction mixture was stirred at room temperature for 15 h. This procedure was adapted from our previous study [15]. The resulting nanoparticles were purified by dialysis as described above. All samples were stored in the dark at 4 °C.

2.4. Synthesis of Schiff base-modified nanoparticles

The aromatic aldehydes (p-anisaldehyde or p-chlorobenzaldehyde) were first dissolved in dimethyl sulfoxide (DMSO) to obtain 25 mM stock solutions. These aldehyde solutions were then added to an aqueous suspension of organosilica nanoparticles at a ratio of 100 μL of aldehyde solution per 1 mL of nanoparticle dispersion, providing an excess relative to the surface amino groups. The reaction mixture was continuously stirred at 45 °C for 6 h to allow Schiff base formation. Upon completion, the modified nanoparticles were purified by dialysis against deionized water, as described above. All synthesized samples were stored in the dark at 4 °C until further use.

2.5. Characterisation of synthesized nanoparticles

2.5.1. Dynamic light scattering

Nanoparticles' size and zeta potential were measured using dynamic light scattering and electrophoretic mobility using the Nano-ZS series instrument (Malvern Instruments, U.K.) at 25 °C. Nanoparticles were dispersed in ultrapure water at the ratio of 1:100 with a refractive index of 1.45 at a scattering angle of 173°. Nanoparticle size is expressed as the mean hydrodynamic diameter ± standard deviation, determined from three independent batches measured in triplicate.

2.5.2. Nanoparticle tracking analysis

Nanoparticle tracking analysis (NTA) was performed using an LM10 instrument equipped with an LM14 laser module and a top plate, operating with a 532 nm green laser (Malvern, UK). As NTA measures the Brownian motion of individual nanoparticles, highly diluted suspensions were required. Therefore, the stock nanoparticle dispersion was diluted 1:10000 prior to measurements. Each diluted sample was loaded into a 1 mL syringe and introduced into the instrument through a syringe pump set at a constant flow rate of 30 a.u. For each sample, five 60-s videos were recorded, and measurements were conducted on three independent samples. Data analysis was carried out using NTA software (version 3.2). All measurements were performed at room temperature (~25 °C) under continuous flow conditions to ensure representative

tracking of the nanoparticle population.

2.5.3. Ellman's assay

The thiol content of the nanoparticles was determined using Ellman's assay [15]. Before analysis, the samples were freeze-dried (Heto Power Dry LL 3000, Thermo Electron Corporation) and dispersed at a concentration of 2 mg/mL in phosphate buffer solution (0.5 mol/L, pH 8). After hydration for 1 h, 500 μL of the nanoparticle dispersion was mixed with 500 μL of DTNB solution (3 mg DTNB in 10 mL of the same buffer) and incubated in the dark for 90 min. The samples were centrifuged at 13000 rpm for 10 min, and the absorbance of the supernatant was measured at 405 nm. Thiol concentration was determined using a cysteine hydrochloride calibration curve (0.020–0.793 μmol/mL), see Fig. S2 in Supplementary information.

2.5.4. 4-Nitrobenzaldehyde assay

A 500 μL silica nanoparticle dispersion was centrifuged for 20 min, and the supernatant was removed [25]. The nanoparticles were redispersed in 1 mL of ethanol with excess of 4-NBA (100-fold amine coverage) and incubated overnight at 45 °C with stirring (1100 rpm). Purification involved four cycles of centrifugation and redispersion in fresh ethanol. The nanoparticles were then incubated in a 1:1 ethanol/water solution at 45 °C overnight, followed by two additional 1-h hydrolysis steps. Optical density at 268 nm confirmed the complete removal of 4-NBA after three cycles. Calibration curves were prepared using 4-NBA standards in hydrolysis solution (0.0078–0.25 μmol/mL), see Fig. S3 in Supplementary information.

2.5.5. Transmission electron microscopy

The morphological characteristics of nanoparticles were examined at electron microscopy facility of Nazarbayev University (Kazakhstan) using transmission electron microscopy (JEOL JEM-1400 Plus). A nanoparticle suspension with a concentration of 1 mg/mL was deposited onto carbon-coated 300-mesh copper grids, with a volume of 8 μL applied to each grid. The grids were air-dried under clean conditions. Samples were visualised at an accelerating voltage of 120 kV.

2.5.6. pH adjustment and measurements

The pH of the nanoparticle dispersions was adjusted by adding small portions of either 1 mol/L HCl or 1 mol/L NaOH. The pH was measured using a pH meter (Seven Direct SD20, Mettler Toledo, Switzerland) at room temperature.

2.5.7. FTIR spectroscopy

Fourier-transform infrared (FTIR) spectra of the freeze-dried nanoparticle samples and their modified forms were recorded using a Vertex 70 V spectrometer (Bruker, Ettlingen, Germany) equipped with a germanium ATR crystal.

2.5.8. Elemental analysis

Elemental composition of the nanoparticles was determined using an Elementar Rapid Micro N Cube analyzer (Langenselbold, Germany). Prior to analysis, the samples were freeze-dried under vacuum. Approximately 1–2 mg of each sample was accurately weighed and sealed in a tin capsule. Each sample was measured in triplicate, and the results are reported as average values.

2.5.9. X-ray diffraction

The crystalline phase composition of the samples was examined by X-ray diffraction (XRD, Tongda TD-3700, China) with Cu Kα radiation (λ_1 =1.54056 Å, λ_2 =1.54439 Å). XRD patterns were collected in the 2θ range of 5–60.

2.6. Toxicological studies

2.6.1. Acute toxicity

Schmidtea mediterranea planaria were maintained and bred in-house in artificial pond water (APW) at room temperature in the dark. They were fed calf liver once per week, and the APW was partially replaced monthly. Artificial pond water was prepared as a mixture of the following salt stock solutions in ultrapure water: 3.2 mL of 5 M NaCl, 10 mL of 1 M $CaCl_2$, 10 mL of 1 M $MgSO_4$, 1 mL of 1 M $MgCl_2$ and 1 mL of 1 M KCl were added to 10 L of ultrapure water, followed by 1.008 g $NaHCO_3$, and the pH was adjusted to 7.0.

Planaria measuring 1.0–1.5 cm in length were placed individually into the wells of 24-well plates, and 2 mL of nanoparticle suspensions (NP, NP-PEG, NP-PEG-AA, and NP-PEG-ChBA) at a concentration of 1 mg/mL were added to each well. A 0.1% (*w/v*) benzalkonium chloride (BAC) solution was used as a positive control, while APW served as the negative control [26,27]. Acute toxicity was assessed over 24, 48, and 72 h by recording the number of live and dead worms. Specimens that showed no movement after gentle agitation of the medium were considered dead.

2.6.2. Planarian toxicity fluorescent assay

The experiment was slightly modified from the procedure previously developed by our group [26]. Following a 24-h treatment with 0.1% of the test substances, the worms were exposed for 1 min to a 0.1% *w/v* sodium fluorescein solution in APW. The excess fluorescein solution was then removed from the planaria by immersing them in APW for 15 min. Each worm was then transferred onto a glass microscope slide and immobilised using several drops of a 2.0% (*w/v*) Type A gelatin solution (Sigma-Aldrich). The slides were placed on ice until the gelatin solidified. Fluorescence images were acquired using a Leica MZ10F stereomicroscope (Leica Microsystems, UK) equipped with a DFC3000G digital camera, under 2.0× magnification, 160 ms exposure time, and a gamma setting of 0.7. All images were analysed in ImageJ software to determine the pixel intensity. Each sample was tested in triplicate, and results were expressed as the mean fluorescence intensity ± standard deviation.

2.7. Antimicrobial effect

2.7.1. The minimum inhibitory concentration

Antimicrobial activity against *Staphylococcus aureus* NCTC 10788 was evaluated in 96-well microplates using the broth microdilution method [28]. Each well was filled with 100 μL of nutrient broth. In the first row, 100 μL of the test sample was added and thoroughly mixed. Then, 100 μL aliquots were transferred sequentially to subsequent wells to obtain two-fold serial dilutions. Amoxicillin solution (40 μg/mL) and nutrient broth without antibiotics served as controls. All wells received 10 μL of a *S. aureus* suspension, resulting in a final inoculum of 5×10^3 CFU/mL.

Plates were covered and sealed with parafilm to prevent evaporation, then incubated at 37 °C for 20 h. After incubation, 20 μL of a 0.02% resazurin solution was added to each well, and plates were further incubated for 1 h. Color change was used to evaluate bacterial viability.

2.7.2. Time-kill kinetic assay

The time-kill kinetic assay was performed according to the method described by Shehabeldine [29] with slight modifications to suit the experimental conditions. *Staphylococcus aureus* NCTC 10788 was grown overnight in a nutrient broth at 37 °C, and the culture was diluted with sterile phosphate-buffered saline (PBS) to obtain an inoculum of approximately 1.6×10^6 CFU/mL. In sterile glass flasks, 500 μL of nutrient broth, 500 μL of the nanoparticle suspension, and 100 μL of the bacterial inoculum were mixed to a total volume of 1.1 mL. The mixtures were incubated at 37 °C with continuous shaking (150 rpm), and aliquots were withdrawn at 0, 3, and 6 h. Each aliquot was serially diluted

in PBS, and 10 μL from each dilution was plated onto nutrient agar plates, which were incubated for 24 h at 37 °C. Viable colonies were counted to determine CFU/mL at each time point. All experiments were carried out in triplicate using independent samples. Data are presented as mean ± standard deviation. Statistical differences between groups were determined using one-way ANOVA.

3. Results and discussion

The thiol–amine bifunctionalized organosilica nanoparticles (OSNPs) were synthesized by co-condensation of (3-mercaptopropyl) trimethoxysilane (MPTS) and (3-aminopropyl)trimethoxysilane (APTS) at a molar ratio of 3:1 using the Ouzo-effect nanoprecipitation approach [24]. The resulting nanoparticles had a mean hydrodynamic diameter of 133 ± 2 nm with a narrow size distribution (PDI < 0.2) and a positive zeta potential of +34 ± 1 mV, indicating the presence of protonated amine groups on the surface. The particles showed good colloidal stability in acidic and near-neutral environments (pH = 3–6); however, at pH > 6, aggregation occurred, as evidenced by a substantial increase in particle size (Fig. 1a). This instability at higher pH is likely attributed to

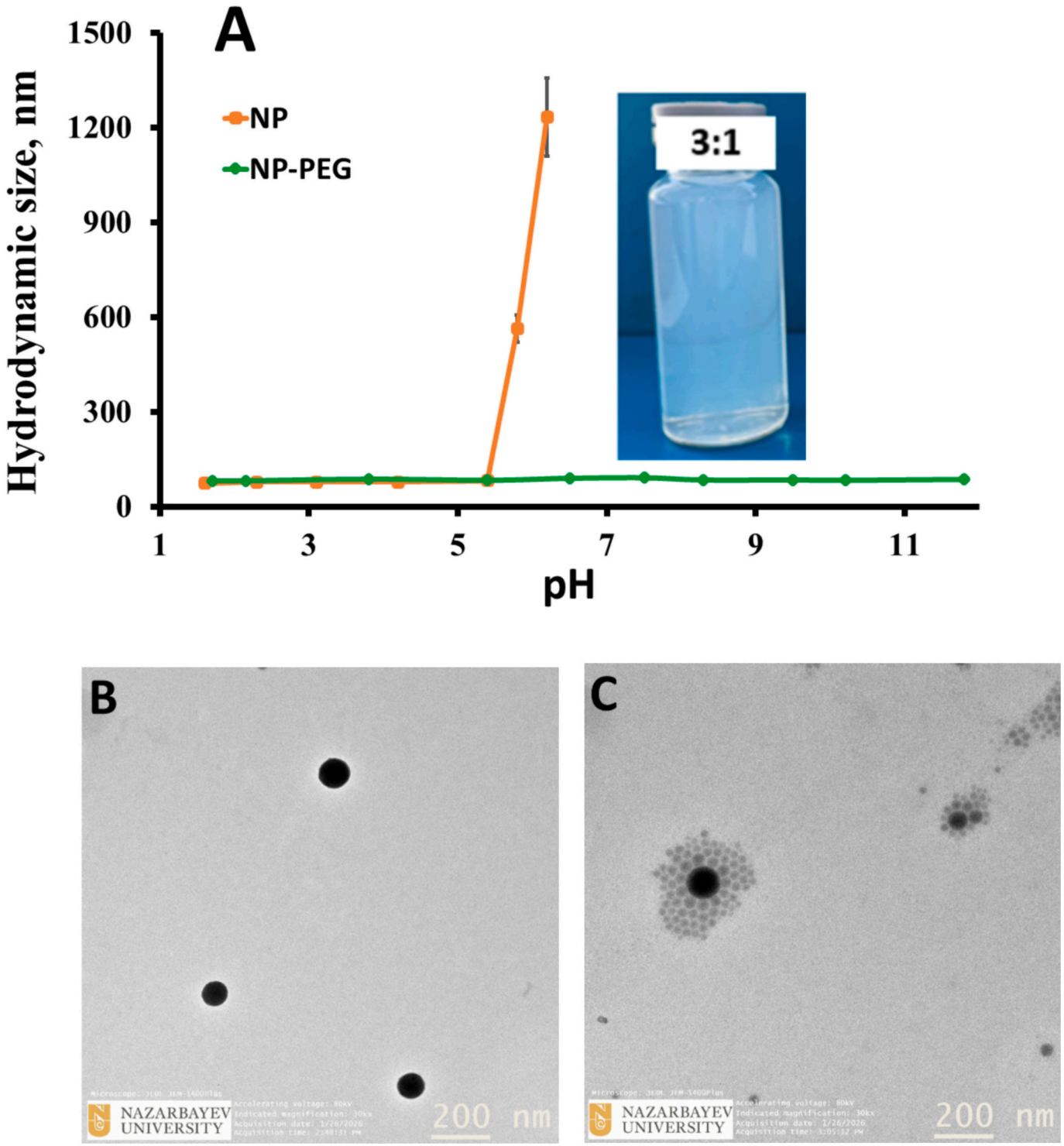

Fig. 1. A) Diameter of nanoparticles in solutions at different pHs. TEM images of B) NP and C) NP-PEG. Some additional TEM images can be found in Fig. S1.

the condensation of surface silanol groups (Si–OH → Si–O–Si) and the deprotonation of amines ($–NH_3^+$ → $–NH_2$), leading to diminished electrostatic repulsion between particles [30,31]. (See Fig. 2.)

The nanoparticles were functionalized with methoxy polyethylene glycol maleimide (MePEG, MW 5000) through thiol–maleimide coupling. After PEGylation, the mean hydrodynamic diameter slightly increased to 142 ± 3 nm, while the zeta potential decreased from +32 ± 1 mV to +11 ± 3 mV, confirming surface modification and the transition from electrostatic to steric stabilization. Quantitative Ellman's assay further confirmed a reduction in surface thiol content from 172 ± 8 μmol/g to 61 ± 57 μmol/g, consistent with PEG grafting onto thiol groups. The content of surface primary amine groups in the initial nanoparticles was determined to be 106 ± 5 μmol/g using the 4-nitrobenzaldehyde assay, providing a reference for subsequent Schiff base formation. The PEGylated OSNPs demonstrated colloidal stability across a wide pH range (1.7–11.8), as the PEG shell effectively prevented aggregation by steric hindrance and reduced oxidation or disulfide cross-linking of thiol groups [32].

Transmission electron microscopy (TEM) was used to examine the morphological characteristics of the thiolated nanoparticles (Fig. 1). The analysis revealed that the nanoparticles were predominantly spherical with an average particle size of 72 ± 13 nm. The particle size determined by TEM was approximately two times smaller than the hydrodynamic diameter obtained by DLS, which may be attributed to differences in the measurement principles of these techniques.

After PEGylation, the nanoparticles were further modified through Schiff base formation with p-anisaldehyde and p-chlorobenzaldehyde. The reaction was performed under mild conditions via condensation between surface amino groups and aldehyde moieties.

DLS measurements showed that the hydrodynamic diameter increased to 159 ± 1 nm for NP-PEG-AA and 158 ± 2 nm for NP-PEG-ChBA, while the zeta potential decreased from +11 mV (NP-PEG) to +7 ± 1 mV and + 8 ± 1 mV, respectively, suggesting successful surface modification and partial neutralization of positively charged amine groups. The slight increase in particle size, combined with the decrease in surface charge, indicates that the modification occurred without aggregation and that the imine formation effectively altered the surface chemistry [32]. The particle sizes measured by DLS and NTA were in good agreement.

To confirm the chemical changes associated with Schiff base formation, the surface primary amine content was quantitatively determined using the 4-nitrobenzaldehyde (4-NBA) assay. The initial organosilica nanoparticles contained 106 ± 5 μmol/g of accessible $–NH_2$ groups (Table 1). After PEGylation, the amount of accessible amine groups decreased to 88 ± 24 μmol/g, which can be attributed to steric shielding of surface functionalities by PEG chains rather than chemical consumption of amines. Following functionalisation with aromatic aldehydes, a further pronounced reduction in accessible amine groups was observed, to 46 ± 11 μmol/g for NP-PEG-AA and 29 ± 16 μmol/g for NP-PEG-ChBA. Based on the difference between the PEGylated and aldehyde-modified samples, approximately 42 ± 26 μmol/g (NP-PEG-AA) and 59 ± 29 μmol/g (NP-PEG-ChBA) of surface amine groups can be considered to have participated in imine bond formation, the formation of Schiff bases [33].

The FTIR spectra of the initial and surface-modified nanoparticles are shown in Fig. 3. In the spectrum of the initial organosilica nanoparticles (NP), absorption bands were observed at 1020 cm^{-1}, 797 cm^{-1} and 559 cm^{-1}, which correspond to ν_{as} (Si–O–Si), ν_s (Si–O–Si) and δ (Si–O–Si) vibrational modes, respectively [20,34]. In addition, absorption bands in the range 3000–2800 cm^{-1} are attributed to the ν (C—H) stretching vibrations of propyl groups, while the bands at 1441 cm^{-1} and 1406 cm^{-1} correspond to δ (C—H) deformation vibrations. A weak band at approximately 1590 cm^{-1} is assigned to the δ (N—H) bending vibrations of surface primary amine groups [35]. In the spectra of PEG-modified nanoparticles, several new absorption bands appeared. In particular, the band at 1708 cm^{-1} corresponds to the carbonyl ν (C=O) stretching vibration of the maleimide fragment and confirms the covalent attachment of PEG–maleimide to the nanoparticle surface. The band at 1465 cm^{-1} is characteristic of CH_2 deformation vibrations in PEG chains, while the signals at 1342 cm^{-1}, 1279 cm^{-1} and 841 cm^{-1} may be associated with ν (C—N) and ν (C–O–C) vibrational modes [36,37]. The aldehyde-modified nanoparticles exhibited new absorption bands in the region associated with the ν (C=N) stretching vibration of Schiff bases. These bands appeared at 1595 cm^{-1} for NP-PEG-AA and at 1619 cm^{-1} for NP-PEG-ChBA, suggesting the formation of imine linkages between the surface amino groups and the aromatic aldehydes [33]. The detailed FTIR band assignments are provided in Table S1. (See Figs. 4 and 5.)

Elemental analysis was employed to monitor changes in the organic composition during the stepwise surface modification of the nanoparticles. The nitrogen content of the amine-functionalized nanoparticles was determined to be 0.37%, confirming the presence of surface amine groups. Following PEGylation with methoxy-poly

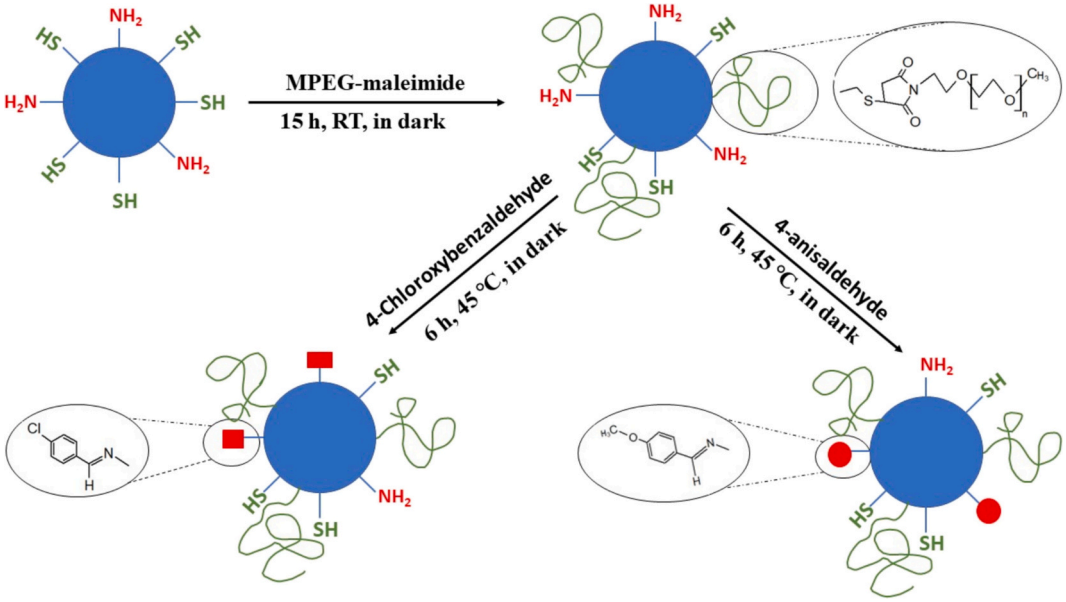

Fig. 2. Schematically illustrates the chemical modifications of the nanoparticles.

Table 1
Physicochemical characteristics of thiol-amine, PEGylated, and aldehyde-modified organosilica nanoparticles.

	Diameter, nm (DLS)	Diameter, nm (NTA)	ξ-potential, mV	PDI	NH_2 groups, μmol/g
NP	133 ± 2	130 ± 2	34 ± 1	0.153 ± 0.002	106 ± 5
NP-PEG	142 ± 3	140 ± 1	11 ± 3	0.208 ± 0.015	88 ± 24
NP-PEG-AA	159 ± 1	162 ± 3	7 ± 1	0.193 ± 0.012	46 ± 11
NP-PEG-ChBA	158 ± 2	161 ± 2	8 ± 1	0.201 ± 0.030	29 ± 16

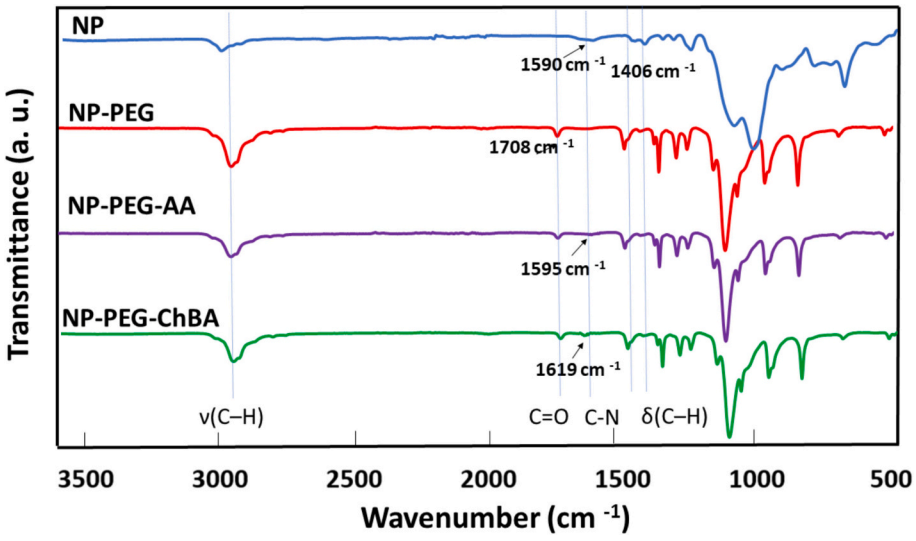

Fig. 3. FTIR spectra of organosilica nanoparticles.

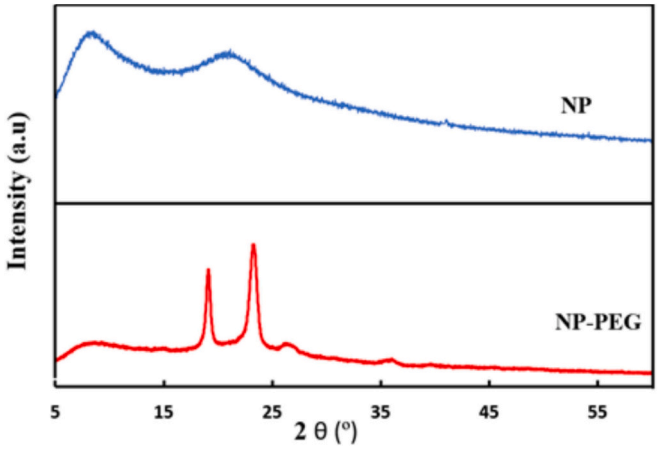

Fig. 4. XRD patterns of unmodified organosilica nanoparticles and PEGylated nanoparticles.

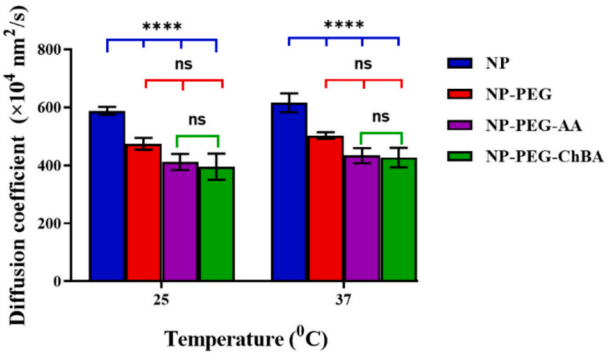

Fig. 5. Diffusion coefficients of unmodified nanoparticles, PEGylated nanoparticles, and aldehyde-modified nanoparticles measured in water at 25 °C and 37 °C. Data show the mean ± standard deviation, where $n = 5$. Statistical significance is indicated as ****$p < 0.0001$, "ns" denotes no significance.

(ethylene glycol) maleimide, the carbon content increased markedly from 19.20% to 40.90%, indicating the successful incorporation of PEG chains onto the nanoparticle surface. Subsequent Schiff base formation with anisaldehyde and chlorobenzaldehyde resulted in further increases in carbon content to 41.07% and 41.12%, respectively. The progressive increase in carbon content is consistent with the stepwise surface functionalization of the silica nanoparticles.

X-ray diffraction (XRD) analysis was performed to evaluate the structural features of the nanoparticles before and after surface modification (Fig. 4). The XRD pattern of the initial organosilica nanoparticles exhibited two broad diffraction halos centered at 2θ ≈ 8.8° and 21.4°. The low-angle is attributed to short-range ordering of organic fragments within the hybrid organosilica network, while the broader halo at ~21° corresponds to the characteristic amorphous Si–O–Si framework [38]. After PEGylation, two additional reflections appeared at 2θ ≈ 19.1° and 23.3°, which are characteristic of semicrystalline PEG domains formed on the nanoparticle surface [39].

To evaluate the influence of surface modification on nanoparticle transport in aqueous media, the diffusion behavior of the nanoparticles was investigated in deionised water using NTA (Table 1). Unmodified nanoparticles exhibited the highest diffusion coefficients at both 25 °C and 37 °C, which is consistent with their smaller hydrodynamic size and the absence of a polymeric shell. PEGylation led to a statistically significant decrease in nanoparticle diffusion ($p < 0.001$). This reduction can be attributed to an increase in hydrodynamic diameter and the formation of a hydrated PEG corona, which enhances frictional resistance and slows particle motion in water. In contrast, further surface modification with aromatic aldehydes did not result in a statistically significant additional change in diffusion compared to NP-PEG. Diffusion coefficients for all nanoparticle formulations increased at 37 °C

compared to 25 °C, reflecting enhanced Brownian motion at elevated temperature [40,41].

3.1. Toxicity

Planaria are aquatic flatworms widely used as model organisms in pharmacological and toxicological research [42–46]. This is attributed to their unique responses to external stimuli, high regenerative capacity, and straightforward maintenance and breeding under laboratory conditions. In this study, the toxicity of nanoparticle suspensions at a concentration of 1 mg/mL (NP, NP-PEG, NP-PEG-AA, and NP-PEG-ChBA) was initially evaluated by incubating *Schmidtea mediterranea* planaria with the tested samples for 24, 48, and 72 h. No mortality was observed at any time point. A 0.1% (*w/v*) benzalkonium chloride (BAC) solution was used as a positive control, while artificial pond water (APW) served as a negative control. Mortality occurred only in the group exposed to BAC.

Previously, [26] reported the development of a planaria-based fluorescent toxicity assay as a rapid and cost-effective pre-screening tool for identifying potential irritants. In the present study, this methodology was used to evaluate the effects of the nanoparticles on the integrity of the planarian epithelial barrier. The assay involves an initial exposure of the worms to solutions of the nanoparticles under investigation, followed by exposure to a sodium fluorescein solution. Disruption of the epithelial barrier results in penetration of the fluorescent dye into the planarian body. As shown in Fig. 6, exposure to all tested nanoparticles at 1 mg/mL did not result in a statistically significant increase in fluorescence intensity compared with the APW control ($p > 0.05$), indicating preservation of epithelial integrity and the absence of irritant effects for both unmodified and modified nanoparticles. In contrast, exposure to 0.1% (*w/v*) BAC, used as a positive control, led to a marked increase in fluorescence intensity ($p < 0.0001$), reflecting epithelial barrier disruption and enhanced dye penetration into planarian tissues.

3.2. Antimicrobial activity

The antimicrobial activity of the nanoparticles was assessed using the broth microdilution method with resazurin as an indicator of bacterial metabolic activity. Resazurin undergoes a color change depending on cell viability: a blue color indicates inhibition of bacterial growth, whereas a pink color reflects active cell proliferation. In the assay, mixtures containing 100 μL of nanoparticle suspension (1 mg/mL) and 100 μL of bacterial suspension were prepared, resulting in a final nanoparticle concentration of 0.5 mg/mL. This corresponded to 29.5 μM for NP-PEG-ChBA and 21 μM for NP-PEG-AA, based on the content of Schiff-base functional groups. After incubation, samples containing nanoparticles modified with aromatic aldehydes exhibited a pronounced blue coloration, indicating effective inhibition of *Staphylococcus aureus* growth (Fig. 7). PEG-modified nanoparticles produced only a slight color change. The lack of activity of the unmodified nanoparticles before their PEGylation is likely due to their aggregation in the nutrient medium (pH = 6.8) (Fig. 1a), which limits their interaction with bacterial cells [19]. The *Staphylococcus aureus* strain used in this study was isolated from a human lesion, underscoring the clinical relevance of the observed antimicrobial effects. Accordingly, mechanisms that reduce microbial load in infection-associated contexts are of particular importance for the development of therapeutic nanomaterials.

Further experiments were conducted to quantitatively evaluate the antimicrobial activity of the nanoparticles using colony-forming unit (CFU) counts (Fig. 8). The initial bacterial concentration prior to nanoparticle exposure was 1.6×10^6 CFU/mL. After 6 h of incubation with the different nanoparticles, bacterial growth was observed in all samples; however, the extent of growth varied markedly between formulations. In the control samples (untreated *Staphylococcus aureus* and PBS dilution), bacterial concentrations reached 4.7×10^9 and 3.8×10^9 CFU/mL, respectively. A statistically significant ($p < 0.05$) but modest reduction in bacterial count was observed in the presence of NP-PEG, which may be attributed to the antibacterial activity of surface-

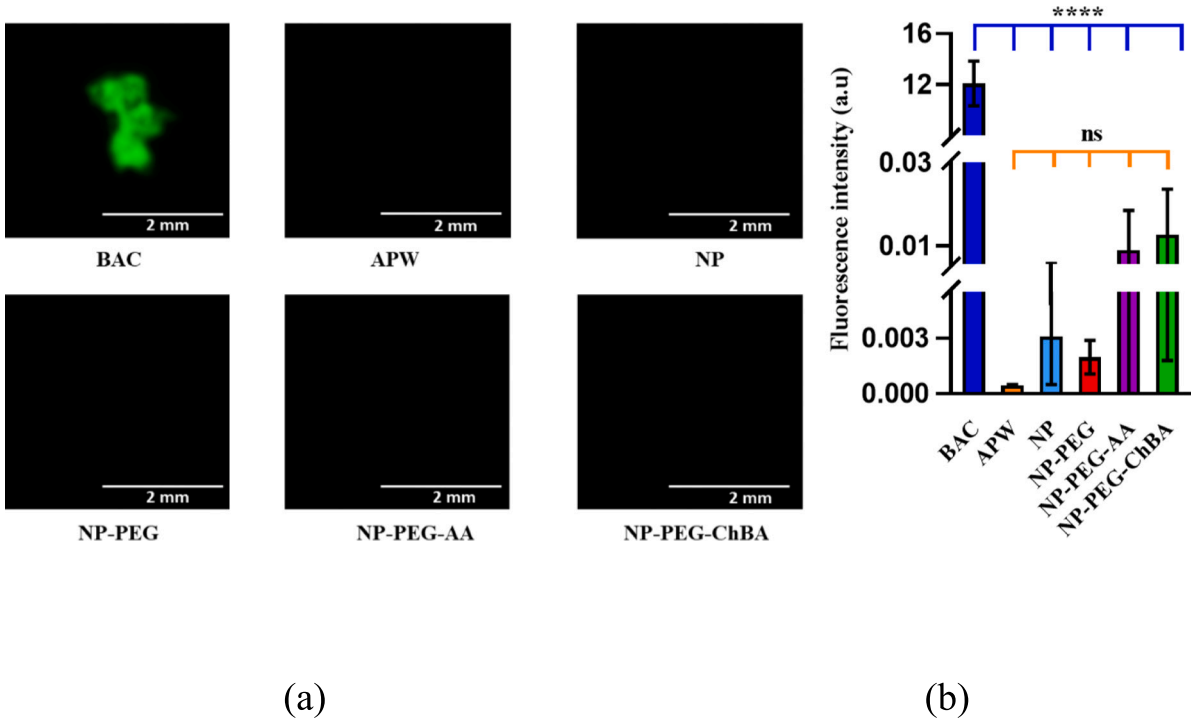

Fig. 6. Fluorescence intensity assay in *Schmidtea mediterranea* planaria: (a) exemplar fluorescence images (scale bar = 2 mm) and (b) fluorescence intensity values after 24-h exposure to 0.1% (w/v) solutions of BAC, APW, and 1 mg/mL suspensions of NP, NP-PEG, NP-PEG-AA, and NP-PEG-ChBA. Each experiment was performed on three individual worms ($n = 3$). Statistical analysis was conducted using one-way ANOVA; **** $p < 0.0001$, ns - no statistically significant difference.

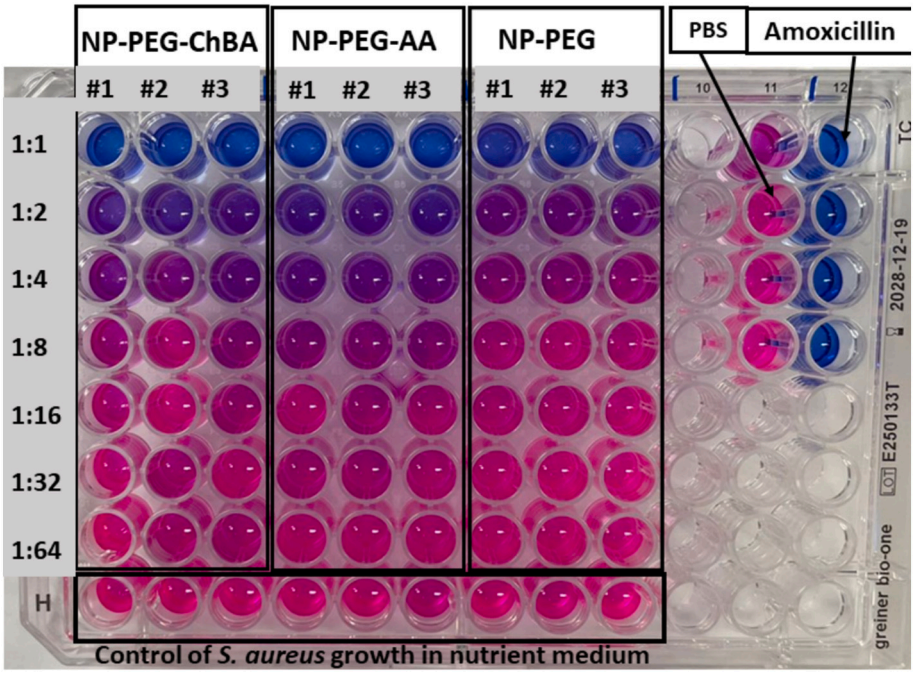

Fig. 7. Images illustrating the evaluation of the antimicrobial activity of NP-PEG-ChBA, NP-PEG-AA, and NP-PEG against *Staphylococcus aureus* NCTC 10788 using the serial dilution assay. PBS and amoxicillin were used as negative and positive controls, respectively. Nanoparticles were tested at an initial concentration of 1 mg/mL, followed by two-fold serial dilutions.

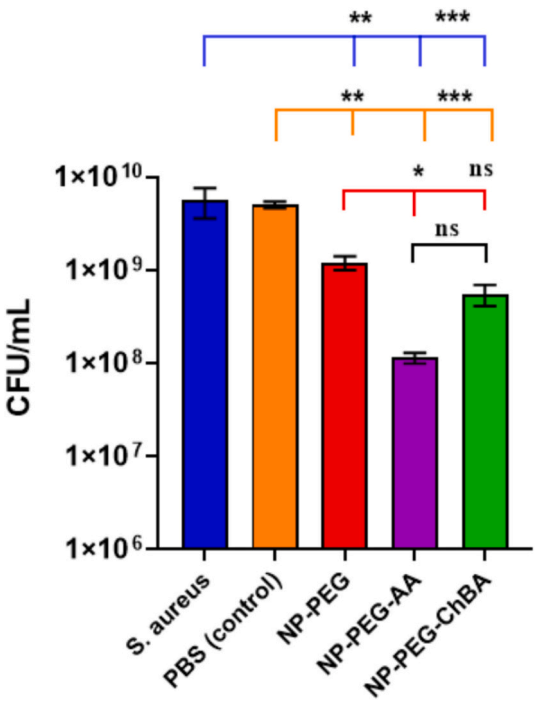

Fig. 8. Concentration of viable *Staphylococcus aureus* NCTC 10788 cells (CFU/mL) after 6 h of incubation at 37 °C in nutrient medium containing PEG-modified nanoparticles and aldehyde-modified nanoparticles, compared with controls (*S. aureus* in nutrient broth and PBS).
ns > 0.05, * $p < 0.05$, ** $p < 0.01$, *** $p < 0.001$; one-way ANOVA.

exposed amino groups. In contrast, a substantial reduction in bacterial counts was detected for nanoparticles modified with aromatic aldehydes, with concentrations decreasing to 1.4×10^8 CFU/mL and 5.9×10^8 CFU/mL in the presence of NP-PEG-AA and NP-PEG-ChBA, respectively. This enhanced antimicrobial activity is likely attributable to the release of p-anisaldehyde and p-chlorobenzaldehyde from the corresponding Schiff bases. Both compounds possess well-documented antibacterial properties [47–49]. The overall increase in bacterial counts relative to the starting concentration likely reflects that the nanoparticle concentration used was insufficient to achieve complete suppression of microbial growth. Many nanoparticle-based and conventional antimicrobial systems do not achieve complete bacterial eradication under moderate doses and short exposure times. Instead, they commonly produce 1–3 log CFU reductions, which are not only statistically significant but also biologically and therapeutically meaningful [50,51]. Such decreases can lower bacterial burden, limit spread, and improve outcomes when combined with complementary therapeutic strategies.

This is consistent with clinical practice. In an ex vivo burn wound model, Chen and co-workers [52] reported that Silvadene (1% silver sulfadiazine) and Flammacerium (1% silver sulfadiazine, 2.2% cerium hexahydrate) typically achieved ~1–3 log reductions across multiple pathogens, whereas mupirocin (a topical antibiotic) produced ~3 log reduction against MRSA (methicillin-resistant *Staphylococcus aureus*). Together, these findings underscore that clinically used topical agents often deliver clinically relevant reductions rather than complete sterilisation.

4. Conclusion

In this study, bifunctional organosilica nanoparticles bearing thiol and amine functionalities were synthesized. Subsequent surface modification with polyethylene glycol and aromatic aldehydes led to the formation of novel functional nanostructures incorporating Schiff-base moieties. Physicochemical characterisation confirmed the preservation of nanoparticle structural integrity and the partial conversion of surface amine groups into imine linkages. The presence of a PEG shell markedly enhanced colloidal stability and effectively suppressed nanoparticle aggregation.

In vivo toxicological studies demonstrated the biocompatibility of the nanoparticles, as none of the tested formulations (NP, NP-PEG, NP-

PEG-AA, and NP-PEG-ChBA) disrupted the epithelial integrity of *Schmidtea mediterranea* planaria or induced observable signs of toxicity. These results confirm that PEGylation enhances both the colloidal stability and biological safety of the nanoparticles in relevant biological environments. Antimicrobial assessment revealed that nanoparticles modified with aromatic aldehydes exhibited inhibitory activity against *Staphylococcus aureus* NCTC 10788. In contrast, PEG-modified nanoparticles showed only weak antimicrobial activity, while unmodified nanoparticles displayed no detectable antimicrobial effect, likely due to aggregation in the nutrient medium.

CRediT authorship contribution statement

Zhansaya E. Kozhantayeva: Writing – original draft, Visualization, Methodology, Investigation, Formal analysis, Data curation. **Gemma Walton:** Writing – review & editing, Resources, Methodology. **Galiya S. Irmukhametova:** Writing – review & editing, Supervision, Resources, Project administration, Funding acquisition. **Vitaliy V. Khutoryanskiy:** Writing – review & editing, Supervision, Resources, Project administration, Funding acquisition, Conceptualization.

Declaration of Generative AI and AI-assisted technologies in the writing process

During the preparation of this work the authors used ChatGPT (OpenAI) to assist with the clarity and flow of some parts of the manuscript. After using this tool/service, the authors reviewed and edited the content as needed and take full responsibility for the content of the publication.

Declaration of competing interest

The authors declare the following financial interests/personal relationships which may be considered as potential competing interests:

Galiya Irmuhametova reports financial support was provided by Ministry of Science and Higher Education of the Republic of Kazakhstan. Vitaliy Khutoryanskiy reports financial support was provided by The Royal Society. If there are other authors, they declare that they have no known competing financial interests or personal relationships that could have appeared to influence the work reported in this paper.

Acknowledgments

The authors acknowledge the Committee of Science of the Ministry of Science and Higher Education of the Republic of Kazakhstan (Grants No. AP26101041 and No. AP19679560) for the financial support of this research. V.V.K. acknowledges the financial support provided by the Royal Society for his Industry Fellowship (IF/R2/222031).

Appendix A. Supplementary data

Supplementary data to this article can be found online at https://doi.org/10.1016/j.bioadv.2026.214795.

Data availability

Data will be made available on request.

References

[1] R.N. Sahoo, S. Rout, A. Parmanik, B.S. Satapathy, S. Pattnaik, L. Maharana, A. K. Nayak, Inorganic biomaterials for ocular drug delivery: a comprehensive review, J. Drug Delivery Sci. Technol. 106 (2025), https://doi.org/10.1016/j.jddst.2025.106667.

[2] Y. Huang, C. Zhang, L. Zhang, X. Chen, W. Fan, Chemical synthesis and multihybridization of small-sized hollow mesoporous Organosilica nanoparticles toward advanced Theranostics, Acc. Chem. Res. 57 (2024) 3465–3477, https://doi.org/10.1021/acs.accounts.4c00502.

[3] S.Yu. Kovtareva, E.E. Kopishev, H. Zhang, S.K. Filippov, Exploring the physicochemical interactions and loading strategies of mesoporous silicon dioxide nanoparticles for drug delivery, Eur. J. Pharm. Biopharm. 208 (2025), https://doi.org/10.1016/j.ejpb.2025.114654.

[4] R. Suryavanshi, K.V. Singh, Fabrication of silica nanoparticles by sol-gel method and effect of TEOS precursor, IOSR Journal of Applied Chemistry (IOSR-JAC) 18 (2025) 12–18, https://doi.org/10.9790/5736-1803011218.

[5] N. Pal, J.-H. Lee, E.-B. Cho, Recent trends in morphology-controlled synthesis and application of mesoporous silica nanoparticles, Nanomaterials 10 (2020), https://doi.org/10.3390/nano10112122.

[6] A.H. Khalbas, T.M. Albayati, N.S. Ali, I.K. Salih, Drug loading methods and kinetic release models using of mesoporous silica nanoparticles as a drug delivery system: a review, S. Afr. J. Chem. Eng. 50 (2024) 261–280, https://doi.org/10.1016/j.sajce.2024.08.013.

[7] R. Fatima, P. Katiyar, K. Kushwaha, Recent advances in mesoporous silica nanoparticle: synthesis, drug loading, release mechanisms, and diverse applications, Front. Nanotechnol. 7 (2025) (2025), https://doi.org/10.3389/fnano.2025.1564188.

[8] N.X.D. Mai, H.-V.T. Nguyen, T.M. Phung, T.M. Le, H.T. Nguyen, L.B. Vong, T.L. H. Doan, Development of amine-functionalized porous organosilica nanoparticles as pH-responsive drug delivery system, J. Drug Delivery Sci. Technol. 89 (2023), https://doi.org/10.1016/j.jddst.2023.104995.

[9] L. Guan, J. Chen, Z. Tian, M. Zhu, Y. Bian, Y. Zhu, Mesoporous organosilica nanoparticles: degradation strategies and application in tumor therapy, VIEW 2 (2021), https://doi.org/10.1002/VIW.20200117.

[10] A.A. Nayl, A.I. Abd-Elhamid, A.A. Aly, S. Bräse, Recent progress in the applications of silica-based nanoparticles, RSC Adv. 12 (2022) 13706–13726, https://doi.org/10.1039/d2ra01587k.

[11] E.D.H. Mansfield, Y. Pandya, E.A. Mun, S.E. Rogers, I. Abutbul-Ionita, D. Danino, A.C. Williams, V.V. Khutoryanskiy, Structure and characterisation of hydroxyethylcellulose-silica nanoparticles, RSC Adv. 8 (2018) 6471–6478, https://doi.org/10.1039/c7ra08716k.

[12] J.H. Al Mahrooqi, V.V. Khutoryanskiy, A.C. Williams, Thiolated and PEGylated silica nanoparticle delivery to hair follicles, Int. J. Pharm. 593 (2021), https://doi.org/10.1016/j.ijpharm.2020.120130.

[13] J.H. Al Mahrooqi, E.A. Mun, A.C. Williams, V.V. Khutoryanskiy, Controlling the size of Thiolated Organosilica nanoparticles, Langmuir 34 (2018) 8347–8354, https://doi.org/10.1021/acs.langmuir.8b01556.

[14] B.A. Zhaisanbayeva, E.A. Mun, L. Ulmanova, Z. Zhunissova, B. Umbayev, F. Olzhayev, I.A. Vorobjev, G. Hortelano, V.V. Khutoryanskiy, In vitro and in vivo toxicity of thiolated and PEGylated organosilica nanoparticles, Int. J. Pharm. 652 (2024), https://doi.org/10.1016/j.ijpharm.2024.123852.

[15] G.S. Irmukhametova, G.A. Mun, V.V. Khutoryanskiy, Thiolated Mucoadhesive and PEGylated Nonmucoadhesive Organosilica nanoparticles from 3-Mercaptopropyltrimethoxysilane, Langmuir 27 (2011) 9551–9556, https://doi.org/10.1021/la201385h.

[16] I. Berger, Z.G. Loewy, Antimicrobial resistance and novel alternative approaches to conventional antibiotics, Bacteria 3 (2024) 171–182, https://doi.org/10.3390/bacteria3030012.

[17] P. Mallari, L.D. Rostami, I. Alanko, F. Howaili, M. Ran, K.K. Bansal, J. M. Rosenholm, O.M.H. Salo-Ahen, The next frontier: unveiling novel approaches for combating multidrug-resistant Bacteria, Pharm. Res. 42 (2025) 859–889, https://doi.org/10.1007/s11095-025-03871-x.

[18] B. Xu, S. Li, R. Shi, H. Liu, Multifunctional mesoporous silica nanoparticles for biomedical applications, Signal Transduct. Target. Ther. 8 (2023), https://doi.org/10.1038/s41392-023-01654-7.

[19] L. Wang, C. Hu, L. Shao, The antimicrobial activity of nanoparticles: present situation and prospects for the future, Int. J. Nanomedicine 12 (2017) 1227–1249, https://doi.org/10.2147/IJN.S121956.

[20] B. de Juan Mora, L. Filipe, A. Forte, M.M. Santos, C. Alves, F. Teodoro, R. Pedrosa, M. Ribeiro Carrott, L.C. Branco, S. Gago, Boosting antimicrobial activity of ciprofloxacin by functionalization of mesoporous silica nanoparticles, Pharmaceutics 13 (2021), https://doi.org/10.3390/pharmaceutics13020218.

[21] F.S. Goharrizi, S.Y. Ebrahimipour, H. Ebrahimnejad, S.J. Fatemi, Magnetic mesoporous silica functionalized with amine groups for efficient removal of heavy metals and bacterial inhibition, J. Clust. Sci. 35 (2024) 2419–2435, https://doi.org/10.1007/s10876-024-02669-y.

[22] Q. Peng, X. Tang, W. Dong, N. Sun, W. Yuan, A review of biofilm formation of *Staphylococcus aureus* and its regulation mechanism, Antibiotics 12 (2023), https://doi.org/10.3390/antibiotics12010012.

[23] S.Y.C. Tong, J.S. Davis, E. Eichenberger, T.L. Holland, V.G. Fowler, Staphylococcus aureus infections: epidemiology, pathophysiology, clinical manifestations, and management, Clin. Microbiol. Rev. 28 (2015) 603–661, https://doi.org/10.1128/CMR.00134-14.

[24] S.J. Chiu, S.Y. Wang, H.C. Chou, Y.L. Liu, T.M. Hu, Versatile synthesis of thiol- and amine-bifunctionalized silica nanoparticles based on the ouzo effect, Langmuir 30 (2014) 7676–7686, https://doi.org/10.1021/la501571u.

[25] Y. Sun, F. Kunc, V. Balhara, B. Coleman, O. Kodra, M. Raza, M. Chen, A. Brinkmann, G.P. Lopinski, L.J. Johnston, Quantification of amine functional groups on silica nanoparticles: a multi-method approach, Nanoscale Adv. 1 (2019) 1598–1607, https://doi.org/10.1039/c9na00016j.

[26] S.I. Shah, A.C. Williams, W.M. Lau, V.V. Khutoryanskiy, Planarian toxicity fluorescent assay: a rapid and cheap pre-screening tool for potential skin irritants, Toxicol. in Vitro 69 (2020), https://doi.org/10.1016/j.tiv.2020.105004.

[27] S. Vanukuru, F. Steele, N.N. Porfiryeva, A. Sosnik, V.V. Khutoryanskiy, Functionalisation of chitosan with methacryloyl and crotonoyl groups as a strategy to enhance its mucoadhesive properties, Eur. J. Pharm. Biopharm. 205 (2024), https://doi.org/10.1016/j.ejpb.2024.114575.
[28] H.M. Hafez, D.H.A. El Hamid, D.T. Fatma Al-Zahraa M. Gomaa, Resazurin microplate assay: rapid assay for detection of methicillin resistant *Staphylococcus aureus*, Int. J. Curr. Microbiol. App. Sci. 6 (2017) 174–181, https://doi.org/10.20546/ijcmas.2017.604.020.
[29] A.M. Shehabeldine, B.H. Amin, F.A. Hagras, A.A. Ramadan, M.R. Kamel, M. A. Ahmed, K.H. Atia, S.S. Salem, Potential antimicrobial and Antibiofilm properties of copper oxide nanoparticles: time-kill kinetic essay and ultrastructure of pathogenic bacterial cells, Appl. Biochem. Biotechnol. 195 (2023) 467–485, https://doi.org/10.1007/s12010-022-04120-2.
[30] L. Bergman, J. Rosenholm, A.-B. Öst, A. Duchanoy, P. Kankaanpää, J. Heino, M. Lindén, On the complexity of electrostatic suspension stabilization of functionalized silica nanoparticles for biotargeting and imaging applications, J. Nanomater. 2008 (2008) 712514, https://doi.org/10.1155/2008/712514.
[31] M. Zienkiewicz-Strzałka, A. Deryło-Marczewska, R.B. Kozakevych, Silica nanocomposites based on silver nanoparticles-functionalization and pH effect, Appl. Nanosci. 8 (2018) 1649–1668, https://doi.org/10.1007/s13204-018-0837-2.
[32] J.S. Suk, Q. Xu, N. Kim, J. Hanes, L.M. Ensign, PEGylation as a strategy for improving nanoparticle-based drug and gene delivery, Adv. Drug Deliv. Rev. 99 (2016) 28–51, https://doi.org/10.1016/j.addr.2015.09.012.
[33] H. Namli, O. Turhan, Background defining during the imine formation reaction in FT-IR liquid cell, Spectrochim. Acta A Mol. Biomol. Spectrosc. 64 (2006) 93–100, https://doi.org/10.1016/j.saa.2005.07.020.
[34] H. Liu, H. Kaya, Y.T. Lin, A. Ogrinc, S.H. Kim, Vibrational spectroscopy analysis of silica and silicate glass networks, J. Am. Ceram. Soc. 105 (2022) 2355–2384, https://doi.org/10.1111/jace.18206.
[35] S. Shahbaz, M. Esmaeili, M.H. Fathian Nasab, Z. Imani, R. Bafkary, M. Amini, F. Atyabi, R. Dinarvand, PEGylated mesoporous silica core–shell redox-responsive nanoparticles for delivering paclitaxel to breast cancer cells, Int. J. Pharm. 655 (2024), https://doi.org/10.1016/j.ijpharm.2024.124024.
[36] E.D.H. Mansfield, K. Sillence, P. Hole, A.C. Williams, V.V. Khutoryanskiy, POZylation: a new approach to enhance nanoparticle diffusion through mucosal barriers, Nanoscale 7 (2015) 13671–13679, https://doi.org/10.1039/c5nr03178h.
[37] C. Malba, U.P. Sudhakaran, S. Borsacchi, M. Geppi, F. Enrichi, M.M. Natile, L. Armelao, T. Finotto, R. Marin, P. Riello, A. Benedetti, Structural and photophysical properties of rare-earth complexes encapsulated into surface modified mesoporous silica nanoparticles, journal of the chemical society, Dalton Trans. 43 (2014) 16183–16196, https://doi.org/10.1039/c4dt00760c.
[38] T. Xiao, M. Yabushita, T. Nishitoba, R. Osuga, M. Yoshida, M. Matsubara, S. Maki, K. Kanie, T. Yokoi, W. Cao, A. Muramatsu, Organic structure-directing agent-free synthesis of Mordenite-type zeolites driven by Al-rich amorphous Aluminosilicates, ACS Omega 6 (2021) 5176–5182, https://doi.org/10.1021/acsomega.0c05059.
[39] B. Van Phuoc, H. Phuong, L.T. Duy Hanh, H.N. Anh Tuan, M.T. Le, N.N. Que Anh, L.T. Thao, G.T. Nguyen, Electro/photo multi-energy triggered expanded graphite/polyethylene glycol composite phase change materials for wearable thermotherapy, RSC Adv. 15 (2025) 29800–29810, https://doi.org/10.1039/d5ra04061b.
[40] E.A. Mun, C. Hannell, S.E. Rogers, P. Hole, A.C. Williams, V.V. Khutoryanskiy, On the role of specific interactions in the diffusion of nanoparticles in aqueous polymer solutions, Langmuir 30 (2014) 308–317, https://doi.org/10.1021/la4029035.
[41] E.D.H. Mansfield, V.R. De La Rosa, R.M. Kowalczyk, I. Grillo, R. Hoogenboom, K. Sillence, P. Hole, A.C. Williams, V.V. Khutoryanskiy, Side chain variations radically alter the diffusion of poly(2-alkyl-2-oxazoline) functionalised nanoparticles through a mucosal barrier, Biomater. Sci. 4 (2016) 1318–1327, https://doi.org/10.1039/c6bm00375c.
[42] L.G. Tunes, J.M. Allen, R.M. Zayas, R.L. do Monte-Neto, Planarians as models to investigate the bioactivity of gold(I) complexes in vivo, Sci. Rep. 8 (2018) 16180, https://doi.org/10.1038/s41598-018-34558-6.
[43] J.-P. Wu, M.-H. Li, The use of freshwater planarians in environmental toxicology studies: advantages and potential, Ecotoxicol. Environ. Saf. 161 (2018) 45–56, https://doi.org/10.1016/j.ecoenv.2018.05.057.
[44] D. Hagstrom, O. Cochet-Escartin, S. Zhang, C. Khuu, E.-M.S. Collins, Freshwater planarians as an alternative animal model for Neurotoxicology, Toxicol. Sci. 147 (2015) 270–285, https://doi.org/10.1093/toxsci/kfv129.
[45] M.M. Habel, A.C. Williams, V.V. Khutoryanskiy, Toxicological assessment of benzalkonium chloride using planaria mobility: a comparison of manual and digital tracking methods, Environ. Toxicol. Pharmacol. 120 (2025), https://doi.org/10.1016/j.etap.2025.104850.
[46] I.S. Thumé, M.E. Frizzo, Sertraline induces toxicity and behavioral alterations in planarians, Biomed. Res. Int. 2017 (2017), https://doi.org/10.1155/2017/5792621.
[47] Y. Adewunmi, S. Namjilsuren, W.D. Walker, D.N. Amato, D.V. Amato, O. V. Mavrodi, D.L. Patton, D.V. Mavrodi, Antimicrobial activity of, and cellular pathways targeted by, *p*-Anisaldehyde and epigallocatechin Gallate in the opportunistic human pathogen Pseudomonas aeruginosa, Appl. Environ. Microbiol. 86 (2020), https://doi.org/10.1128/AEM.02482-19 e02482–19.
[48] M.A.F. Mohamed, I. Benjamin, G.A. Okon, I. Ahmad, S.A.P.M. Khan, H. Patel, E. C. Agwamba, H. Louis, Insights into in-vitro studies and molecular modelling of the antimicrobial efficiency of 4-chlorobenzaldehyde and 4-methoxybenzaldehyde derivatives, J. Biomol. Struct. Dyn. 42 (2024) 6042–6064, https://doi.org/10.1080/07391102.2023.2239917.
[49] E. Soliman, S. El-Kousy, H. Abd-Elbary, A. Abou-zeid, Low molecular weight chitosan-based Schiff bases: synthesis, characterization and antibacterial activity, Am. J. Food Technol. 8 (2013) 17–30, https://doi.org/10.3923/ajft.2013.17.30.
[50] A. Masri, D.M. Brown, D.G.E. Smith, V. Stone, H.J. Johnston, Comparison of in vitro approaches to assess the antibacterial effects of nanomaterials, J. Funct. Biomater. 13 (2022), https://doi.org/10.3390/jfb13040255.
[51] S. Hawas, A.D. Verderosa, M. Totsika, Combination therapies for biofilm inhibition and eradication: a comparative review of laboratory and preclinical studies, Front. Cell. Infect. Microbiol. 12 (2022), https://doi.org/10.3389/fcimb.2022.850030.
[52] P. Chen, E.A. Sebastian, S.L.R. Karna, K.P. Leung, Development of a stringent ex vivo-burned porcine skin WoundModeltoScreen topical antimicrobial agents, Antibiotics 13 (2024) 1159, https://doi.org/10.3390/antibiotics13121159.